Transferred, Ultrathin Oxide Bilayers as Biofluid Barriers for Flexible Electronic Implants

*Enming Song, Yoon Kyeung Lee, Rui Li, Jinghua Li, Xin Jin, Ki Jun Yu, Zhaoqian Xie, Hui Fang, Yiding Zhong, Haina Du, Jize Zhang, Guanhua Fang, Yerim Kim, Younghee Yoon, Muhammad A. Alam, Yongfeng Mei, Yonggang Huang, and John A. Rogers**

The work presented here introduces a materials strategy that involves physically transferred, ultrathin layers of silicon dioxide (SiO_2) thermally grown on silicon wafers and then coated with hafnium oxide (HfO_2) by atomic layer deposition, as barriers that satisfy requirements for even the most challenging flexible electronic devices. Materials and physics aspects of hydrolysis and ionic transport associated with such bilayers define their performance and reliability characteristics. Systematic experimental studies and reactive diffusion modeling suggest that the HfO_2 film, even with some density of pinholes, slows dissolution of the underlying SiO_2 by orders of magnitude, independent of the concentration of ions in the surrounding biofluids. Accelerated tests that involve immersion in phosphate-buffered saline solution at a pH of 7.4 and under a constant electrical bias demonstrate that this bilayer barrier can also obstruct the transport of ions that would otherwise cause drifts in the operation of the electronics. Theoretical drift–diffusion modeling defines the coupling of dissolution and ion diffusion, including their effects on device lifetime. Demonstrations of such barriers with passive and active components in thin, flexible electronic test structures highlight the potential advantages for wide applications in chronic biointegrated devices.

1. Introduction

Emerging classes of flexible hybrid electronics/optoelectronic devices offer attractive capabilities as active interfaces to biological systems of relevance to both clinical practice and biomedical research. Associated embodiments range from flexible filaments for optoelectronic stimulation of targeted neural circuits in the brain,[1–4] to conformal sheets for high-resolution multiplexed electrophysiological mapping on the epicardial surfaces.[5–9] Such platforms are of great interest because they can form minimally invasive interfaces to dynamic, soft biological systems, while providing performance characteristics that can approach those of conventional, wafer-based semiconductor devices.[10–20] A critical challenge in this field is in the development of materials that, in flexible, thin film form, can simultaneously serve as perfect barriers

E. Song, Prof. Y. Mei
Department of Materials Science
Fudan University
Shanghai 200433, P. R. China

E. Song, Y. K. Lee, Dr. J. Li, Y. Zhong, H. Du, J. Zhang, G. Fang, Y. Kim, Y. Yoon
Frederick Seitz Materials Research Laboratory
Department of Materials Science and Engineering
Department of Chemistry
University of Illinois at Urbana-Champaign
Urbana, IL 61801, USA

Prof. R. Li
State Key Laboratory of Structural Analysis for Industrial Equipment
Department of Engineering Mechanics
International Research Center for Computational Mechanics
Dalian University of Technology
Dalian 116024, P. R. China

X. Jin, Prof. M. A. Alam
School of Electrical and Computer Engineering
Purdue University
West Lafayette, IN 47907, USA

Dr. K. J. Yu
School of Electrical and Electronic Engineering
Yonsei University
Seoul 03722, Republic of Korea

Dr. Z. Xie
AML, Department of Engineering Mechanics
Center for Mechanics and Materials
Tsinghua University
Beijing 100084, China

Dr. Z. Xie, Prof. Y. Huang
Department of Mechanical Engineering
Department of Civil and Environmental Engineering
and Department of Materials Science and Engineering
Northwestern University
Evanston, IL 60208, USA

Dr. H. Fang
Department of Electrical and Computer Engineering
Northeastern University
Boston, MA 02115, USA

DOI: 10.1002/adfm.201702284

to biofluids and as high-quality interfaces to the surrounding biology with multidecade lifetimes.

An ideal material for this purpose must be biocompatible, with both exceptionally low flexural rigidity and water/ion permeability. Conventional encapsulation strategies, ranging from bulk metal/ceramic enclosures in standard implantable devices to organic/inorganic multilayer stacks in organic light emitting diode displays, fail, typically by orders of magnitude, to simultaneously meet both of these latter two critical requirements.[21–27] Even for materials that have minimal permeability, challenges in forming perfect, pinhole-free coatings over large areas can be difficult or impossible to overcome, particularly in academic laboratory conditions. A recently reported solution involves a physically transferred layer of SiO_2 thermally grown on a pristine silicon wafer. Results indicate extraordinary water barrier properties at thicknesses that allow both compliant mechanics and a high capacitance electrical measurement interface.[28] Due to its extremely low water permeability and pinhole-free nature, this type of barrier offers key advantages over conventional coatings, as extrapolated from temperature-dependent studies of immersion in phosphate-buffered saline (PBS) solution. Additionally, the nature of the growth process and the transfer procedures eliminate the need for particulate-free fabrication environments. System demonstrators exploit 1-μm-thick layers of transferred thermal SiO_2 as water barriers and capacitive measurement interfaces in which backplanes of flexible silicon electronics provide amplification and multiplexed addressing for in vivo electrophysiological mapping on the brain and heart.[29]

An intrinsic limitation of this strategy is that the rates for hydrolysis of thermal SiO_2 (0.04 nm d^{-1} at 37 °C; ≈90 nm d^{-1} at 96 °C) limit the ability to exploit ultrathin film geometries (e.g., 100 nm thick) for enhanced capacitive coupling. Also, ions commonly present in biofluids, particularly sodium, can diffuse through thermal SiO_2 where they can shift and/or degrade the switching properties of the underlying transistors. The addition of silicon nitride can mitigate the diffusion issue, but its rate of hydrolysis exceeds that of SiO_2,[30] thereby requiring its use as an underlayer, away from the biofluid interface.

Here, we present materials, designs, and integration strategies for an ultrathin, transferred barrier that combines thermally grown SiO_2 with a coating of HfO_2 formed by atomic layer deposition (ALD). By comparison to previous work on single-layer systems of thermal SiO_2, systematic experimental studies and reactive diffusion modeling suggest that this bilayer barrier can offer significantly enhanced longevity for underlying flexible electronics, at ultrathin geometries. Accelerated immersion tests demonstrate that the HfO_2 slows the dissolution of the underlying SiO_2 in simulated biofluids by orders of magnitude, even when present with some density of pinholes. Additional results establish aspects of ionic transport through such materials via measurements of electrostatically induced shifts in the electrical properties of the underlying transistors. A combination of soak tests and temperature-dependent simulations provides foundational understanding of the role of two competing failure mechanisms—dissolution and ion diffusion—on device lifetime. The findings indicate that this bilayer barrier offers excellent capabilities of relevance to a diverse range of biointegrated flexible electronic devices.

2. Results and Discussion

Standard semiconductor processing strategies in growth and transfer printing enable the fabrication of high-quality electronics directly on oxide layers as barriers to biofluids (**Figure 1**a). The scheme used here combines some aspects of conventional strategies in which deposition of encapsulation material occurs as a last step, with more recently reported alternatives in which device processing occurs in a layer-by-layer fashion on a preformed barrier layer. Figure 1a outlines the four main steps. Briefly, electronic devices formed on an ultrathin layer of thermal SiO_2 on a silicon wafer transfer, with the SiO_2, onto a flexible plastic substrate. Subsequently, deposition of HfO_2 by ALD forms a capping layer on the top, exposed surface of the SiO_2. For the studies reported here, the electronics consist of an array of transistors formed on a silicon-on-insulator (SOI) wafer (≈100-nm-thick device Si and 300-nm-thick buried thermal SiO_2) with the device Si (silicon nanomembranes, Si NMs) as the active channel material. The transfer process bonds the front side of the wafer to a thin polyimide film laminated on a glass plate as a temporary support. Inductively coupled plasma reactive ion etching removes the silicon wafer and simultaneously reduces the buried thermal SiO_2 thickness to 100 nm, as shown in the Appendix and Figure S1 (Supporting Information). Peeling the device from the glass after depositing HfO_2 (100 nm thick, by a rate of 1.07 Å $cycle^{-1}$ in 200 °C) by ALD on the SiO_2 yields a piece of flexible electronics encapsulated by an ultrathin bilayer barrier of HfO_2/SiO_2. Details appear in the Experimental Section. Such devices, by virtue of their small combined thicknesses, exhibit excellent mechanic flexibility in cyclic bending tests (see details in the Appendix and Figure S2, Supporting Information). Recent work demonstrates that SiO_2 formed and processed in similar fashion can serve as front and back side encapsulation for flexible, actively multiplexed electrophysiological mapping systems.[28] The two upper insets of Figure 1b are optical images of flexible electronics with a set of NMOS transistors (channel length L = 20 μm, width W = 200 μm). The bilayer barrier consists of a 100-nm-thick capping layer of ALD HfO_2 (biofluids side) and 100-nm-thick underlying layer of thermal SiO_2 (device side), as illustrated in the lower inset.

Results of accelerated soak tests of NMOS transistors while immersed in PBS solution with a pH of 7.4 at a temperature of

Prof. J. A. Rogers
Department of Materials Science and Engineering
Department of Biomedical Engineering
Department of Neurological Surgery
Department of Chemistry
Department of Mechanical Engineering
Department of Electrical and Computer Science
Center for Bio-Integrated Electronics
Simpson Querrey Institute for Nano/biotechnology
Northwestern University
Evanston, IL 60208, USA
E-mail: jrogers@northwestern.edu

The ORCID identification number(s) for the author(s) of this article can be found under https://doi.org/10.1002/adfm.201702284.

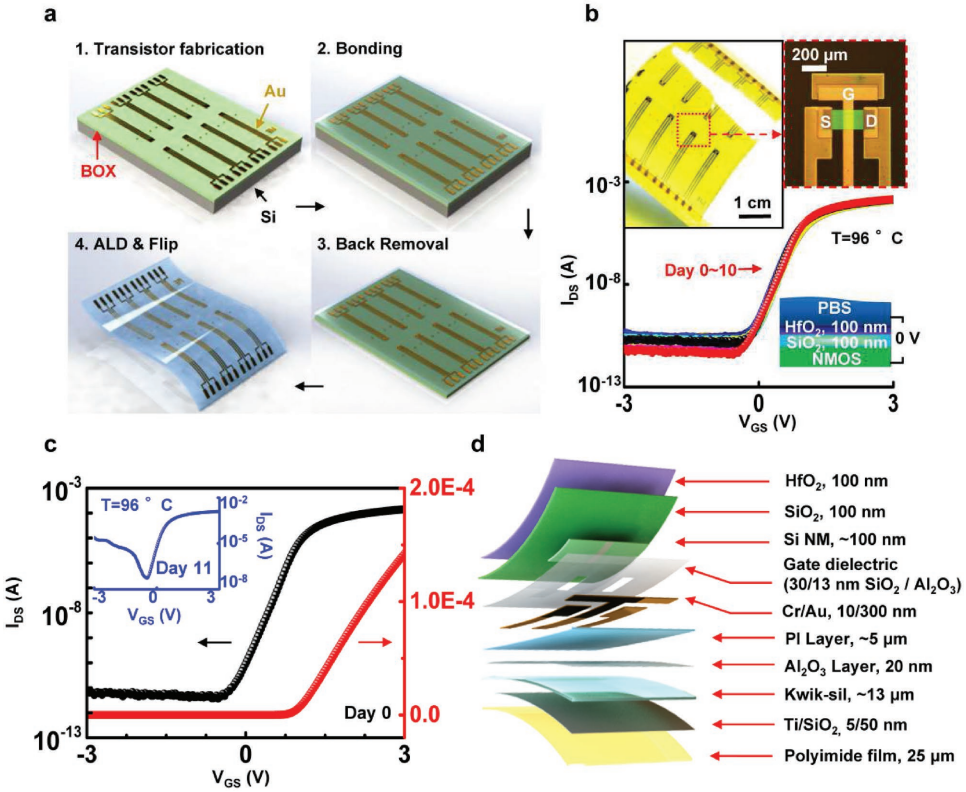

Figure 1. Transferred, ultrathin bilayer of SiO_2 thermally grown on silicon wafers and HfO_2 formed by ALD serve as excellent barriers to biofluids and ions in flexible electronic implants. a) Scheme for fabricating test structures that include silicon transistors: 1) Fabrication of transistors on an SOI wafer; 2) Pressure bonding the top surface of this wafer, face down, onto to a glass substrate that is laminated with a thin film of polyimide (Kapton, 13 μm); 3) Removal of the silicon handle wafer by dry etching; 4) Surface cleaning and ALD of HfO_2; release of the flexible device from the substrate. b) Transfer characteristics collected during immersion in PBS solution at pH 7.4 and 96 °C for 10 d, at a supply voltage $V_{DS} = 0.1$ V. The upper insets show optical images of a sample produced in this manner with a 100/100-nm-thick bilayer of HfO_2/SiO_2 as a barrier on its top surface and a single transistor structure after bonding. The lower inset shows a schematic illustration of the NMOS transistor stack. c) Transfer characteristics at Day 0 plotted in both linear and semilog scales, at a supply voltage $V_{DS} = 0.1$ V. The inset shows transfer characteristics collected at the time of failure on Day 11. d) Schematic illustration of the material stack at the location of an NMOS transistor.

96 °C are in Figure 1b, in the form of transfer characteristics of a representative transistor at a supply voltage $V_{DS} = 0.1$ V. Here, the accelerated tests refer to those performed at elevated temperatures to increase the rate of the hydrolysis reaction. At Day 0, Figure 1c demonstrates the transfer characteristics in both linear and semilog scales. The on/off current ratio is ≈10^8 and the peak effective electron mobility is ≈400 $cm^2\ V^{-1}\ s^{-1}$ (see Supporting Information). All transistors exhibit stable performance for 10 d (Figure 1b) until a sudden failure at Day 11 (inset of Figure 1c). Previous research indicates that although the water permeability through thermal SiO_2 is extremely small, a slow hydrolysis process ($SiO_2 + 2H_2O \rightarrow Si(OH)_4$, corresponding to a dissolution rate of ≈90 nm d^{-1} in 96 °C PBS solution at a pH of 7.4) consumes the material, thereby leading to eventual failure. By comparison, a 100/100-nm-thick bilayer of HfO_2/SiO_2 barrier has a lifetime ≈10 times longer than that of an isolated 100-nm-thick layer of thermal SiO_2 barrier (≈1 d in the same condition, consistent with the dissolution rate of ≈90 nm d^{-1} in previous report), as displayed in the Appendix and Figure S3a (Supporting Information). A single layer of HfO_2 (100 nm thick) fails quickly due to a small, but finite density of pinholes, as in the Appendix and Figure S3b (Supporting Information). As a result, the HfO_2/SiO_2 bilayer, in which the HfO_2 slows the dissolution of the SiO_2 and the SiO_2 forms a defect-free barrier, can provide an attractive solution to the challenge of chronic encapsulation of thin, flexible electronics. A corresponding schematic illustration of the multilayer configuration is shown in Figure 1d, as an exploded view.

Soak tests using setups that incorporate thin films of magnesium (Mg), as in **Figure 2**, instead of transistors can facilitate rapid evaluation of various water barriers. The strong reactivity of Mg with water ($Mg + 2H_2O \rightarrow Mg(OH)_2 + H_2$) leads, upon exposure, to defects that are immediately and easily visible by optical microscopy. Here, a 200 × 400 μm^2 pad of 300-nm-thick layer of Mg deposited by electron-beam evaporation serves, in this manner, as a water-penetration sensor to test the barrier properties of different layers deposited or transferred on top. Figure 2a shows a schematic illustration of a test setup (Figure 2b), for which accelerated testing involves continuous immersion in PBS solution at 96 °C. For present purposes, the barrier lifetime corresponds to the period between immersion and the appearance of the first defect observable on the Mg pad by optical microscopy. This criteria has practical value because the lifetimes (days) for systems of interest here are much longer

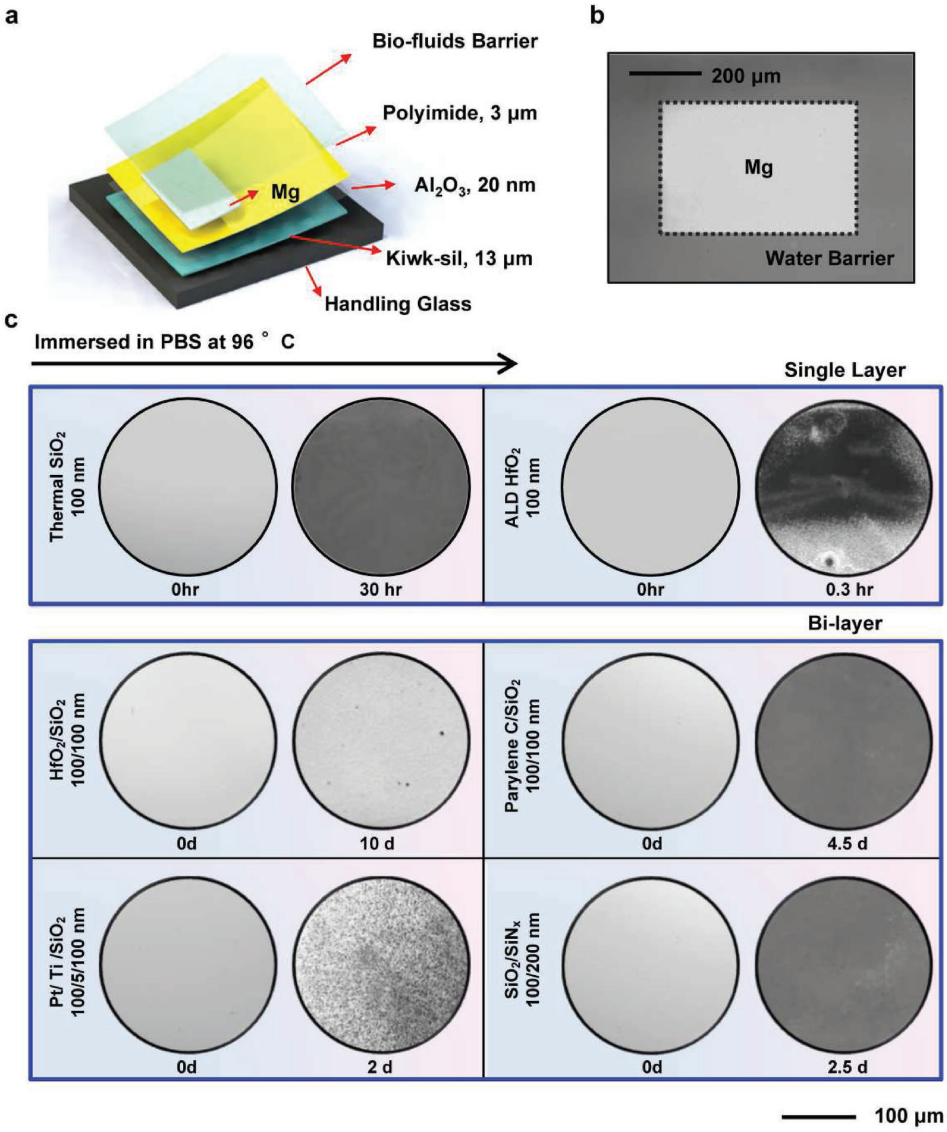

Figure 2. Effects of the capping layer thickness and materials type on the rate of dissolution of SiO_2. a) Illustration of the layer configuration for tests that use thin films of Mg as indicators of water penetration. b) Top-view optical image of a Mg pad encapsulated by a barrier layer. c) Results of accelerated immersion tests that involve immersion in PBS solution at 96 °C. The single-layer row displays findings for 100-nm-thick layers of SiO_2 and HfO_2 as barriers, respectively. The double-layer rows show sequential images of Mg encapsulated by various capping layers on SiO_2, including HfO_2, Parylene C, Ti/Pt, and LPCVD SiN_x.

than the time (minutes to hours) for an initial defect in the Mg pad to propagate laterally across its entire spatial extent. As a result, uncertainties in the time to identify the first observable defect are much smaller than the lifetime itself.

As shown in the single-layer row in Figure 2c, the device encapsulated by a 100-nm-thick layer of thermal SiO_2 survives for 30 h, after which time the entire Mg layer dissolves at once, in a "bulk" mode, by consequence of the spatially uniform dissolution of SiO_2, at a consistent rate of ≈90 nm d^{-1} at 96 °C (0.04 nm d^{-1} at 37 °C)[28] and its pinhole free nature. The addition of a layer of HfO_2, which itself is insoluble in water (inset of the Appendix and Figure S4, Supporting Information) and simultaneously is nontoxic and biocompatible,[31,32] can dramatically increase the time for failure of the SiO_2 layer by hydrolysis. The main limitation of using HfO_2 alone is the nearly unavoidable formation of pinholes or other defects across the area of interest during deposition in the type of cleanroom environments available to academic labs. Under our experimental conditions, degradation of Mg with a single layer of HfO_2 as a barrier occurs in a very short time in Figure 2c (see also Figure S4, Supporting Information) due to these defects. Nevertheless, diffusion of water through the HfO_2 can be significantly impeded, with consequent reductions on the rate of dissolution of the underlying SiO_2.

These observations motivate the use of a bilayer barrier that combines thermal SiO_2 (device side) and HfO_2 (contact with PBS). The SiO_2 serves as a water-impermeable barrier without defects, and HfO_2 serves as an insoluble, capping layer that

slows the dissolution of the SiO_2. The HfO_2/SiO_2 (100/100 nm thick) bilayer, as shown in the second row of Figure 2c, leads to isolated defects in the Mg pad after 10 d, which then expand to consume the entire layer of Mg in a few hours (consistent with active-transistor results in Figure 1b). Here, isolated visible defects in the Mg appear at a density of 3–4 per pad (200×400 μm^2). As a result, the HfO_2/SiO_2 bilayer barrier eventually fails due to dissolution through these pinholes (see details in the Figure S5, Supporting Information). Experiments performed in the same manner but with various other capping materials provide points of comparison. Other metal-oxide layers, for example, Al_2O_3 or TiO_2, show inferior barrier properties compared HfO_2 (Appendix and Figure S6, Supporting Information) due to correspondingly higher densities of pinholes. Polymers, for example, lead to Mg degradation in a 'bulk' mode, associated with water permeation across the entire area (see the Appendix and Table S1, Supporting Information). Others, such as platinum/titanium, display more severe pinhole issues and much shorter lifetimes compared to the bilayer barrier of HfO_2/SiO_2. Another possibility is SiN_x, but its dissolution rate in PBS solution surpasses that of thermal SiO_2 by orders of magnitude.[30] As shown in Figure 2c, the performance of HfO_2/SiO_2 bilayer barrier is superior to all other combinations explored, due to a combination of low water diffusivities, small pinhole densities, and low effective dissolution rates for HfO_2.

Figure 3 shows results of theoretical modeling of reactive diffusion in thermal SiO_2 and HfO_2/SiO_2 in PBS solution. A 1D single-layer model captures dissolution of thermal SiO_2, without any capping layer, since the initial thickness h_0 is much smaller than the lateral dimensions.[33] Figure 3a presents a schematic illustration of the model, where y denotes the thickness direction, with $y = 0$ at the bottom of the layer. The governing equation is[34]

$$D_{SiO_2}\frac{\partial^2 w}{\partial y^2} - k_{SiO_2} w = \frac{\partial w}{\partial t},\ 0 \le y \le h_0 \tag{1}$$

where D_{SiO_2} and k_{SiO_2} are the diffusivity of water and the reaction constant between the SiO_2 and water, respectively, w is the water concentration, which depends on position y and time t. The boundary conditions can be written as $w|_{y=h_0} = w_0$ and $\partial w/\partial y|_{y=0} = 0$, corresponding to a water concentration that is constant w_0 (= 1 g cm^{-3}) at the water/SiO_2 interface and a water flux at the bottom surface of the thermal SiO_2 layer that is zero. The initial condition is zero water concentration in the thermal SiO_2, that is, $w|_{t=0} = 0$ ($0 \le y < h_0$). The water concentration can be analytically solved by applying the method of separation of variables, which gives the thickness h_{SiO_2} of the thermal SiO_2 layer as a function of time (details appear in the Appendix, Supporting Information). For the present study

$$\frac{h_{SiO_2}}{h_0} \approx 1 - \frac{t}{t_{critical}} \tag{2}$$

where

$$t_{critical} = \frac{h_0 q \rho_{SiO_2} M_{H_2O}}{w_0 M_{SiO_2}\sqrt{k_{SiO_2} D_{SiO_2}}\tanh\sqrt{\frac{k_{SiO_2} h_0^2}{D_{SiO_2}}}} \tag{3}$$

is the critical time for full dissolution of the thermal SiO_2. Here, q (= 2) is the number of water molecules that react with each atom of SiO_2, ρ_{SiO_2} is the mass density of thermal SiO_2 (= 2.33 g cm^{-3}), M_{SiO_2} (= 60 g mol^{-1}) and M_{H_2O} (= 18 g mol^{-1}) are the molar masses of SiO_2 and water, respectively.

From soak tests of thermal SiO_2 in PBS solution, the diffusivity D_{SiO_2} and reaction constant k_{SiO_2} can be extracted using this model as $D_{SiO_2} = 1.5 \times 10^{-16}$ cm^2 s^{-1} and $k_{SiO_2} = 2 \times 10^{-4}$ s^{-1} at 96 °C. These values fall within the range of those inferred from previous studies for PECVD SiO_2 ($k = 5.3 \times 10^{-5}$ to 8.1×10^{-3} s^{-1})[33] and silica glass ($D = 2.1 \times 10^{-18}$ to 1.3×10^{-14} cm^2 s^{-1}).[35,36] The two constants at the other temperatures can be inferred from those at 96 °C by experimentally measured dissolution rates and the Arrhenius equation, with an apparent activation energy $E_A = 1.32$ eV (details appear in the Appendix, Supporting Information).[28] Figure 3b shows the change in the thickness of the thermal SiO_2 with time in PBS solution at 96 °C. The simulated results (lines) agree well with those measured (symbols; Mprobe Station, SemiconSoft, USA) for all three initial thicknesses, that is, 30, 50, and 75 nm. For a layer of ALD HfO_2 submerged in PBS solution, experiments show that the thickness does not change with time (inset of Figure S4, Supporting Information), indicating that the reaction constant between HfO_2 and water is zero.

A bilayer model for the case of HfO_2/SiO_2 is in Figure 3c. For the thermal SiO_2, the reactive diffusion Equation (1), as well as the boundary condition $\partial w/\partial y|_{y=0} = 0$ and initial condition $w|_{t=0} = 0$, still apply. For the HfO_2 layer, the diffusion equation is

$$D_{HfO_2}\frac{\partial^2 w}{\partial y^2} = \frac{\partial w}{\partial t}\quad \left(h_0 \le y \le h_0 + h_{HfO_2}\right) \tag{4}$$

with the boundary condition $w|_{y=h_0+h_{HfO_2}} = w_0$ and initial condition $w|_{t=0} = 0$ ($h_0 \le y \le h_0 + h_{HfO_2}$), where D_{HfO_2} is the diffusivity of water in HfO_2. The continuity of concentration and flux of water at the HfO_2/SiO_2 interface requires $w|_{y=h_0-0} = w|_{y=h_0+0}$ and $D_{SiO_2}\,\partial w/\partial y|_{y=h_0-0} = D_{HfO_2}\,\partial w/\partial y_{y=h_0+0}$. By applying the method of separation of variables, an analytical solution for the water concentration for this bilayer model can be obtained, which gives the thickness of the thermal SiO_2 layer (details appear in the Appendix, Supporting Information). For the present study

$$\frac{h_{SiO_2}}{h_0} \approx 1 - \frac{t}{t'_{critical}} \tag{5}$$

where

$$t'_{critical} = \alpha t_{critical} \tag{6}$$

represents the time when the thermal SiO_2 layer completely disappears ($h_{SiO_2} = 0$), that is, the lifetime of the HfO_2/SiO_2 bilayer barrier. Here

$$\alpha = 1 + \sqrt{D_{SiO_2} k_{SiO_2}}\,\frac{h_{HfO_2}}{D_{HfO_2}}\tanh\sqrt{\frac{k_{SiO_2} h_0^2}{D_{SiO_2}}} \tag{7}$$

From soak tests, the diffusivity D_{HfO_2} is determined from the bilayer model as $D_{HfO_2} = 2.5 \times 10^{-16}$ cm^2 s^{-1} at 96 °C. For

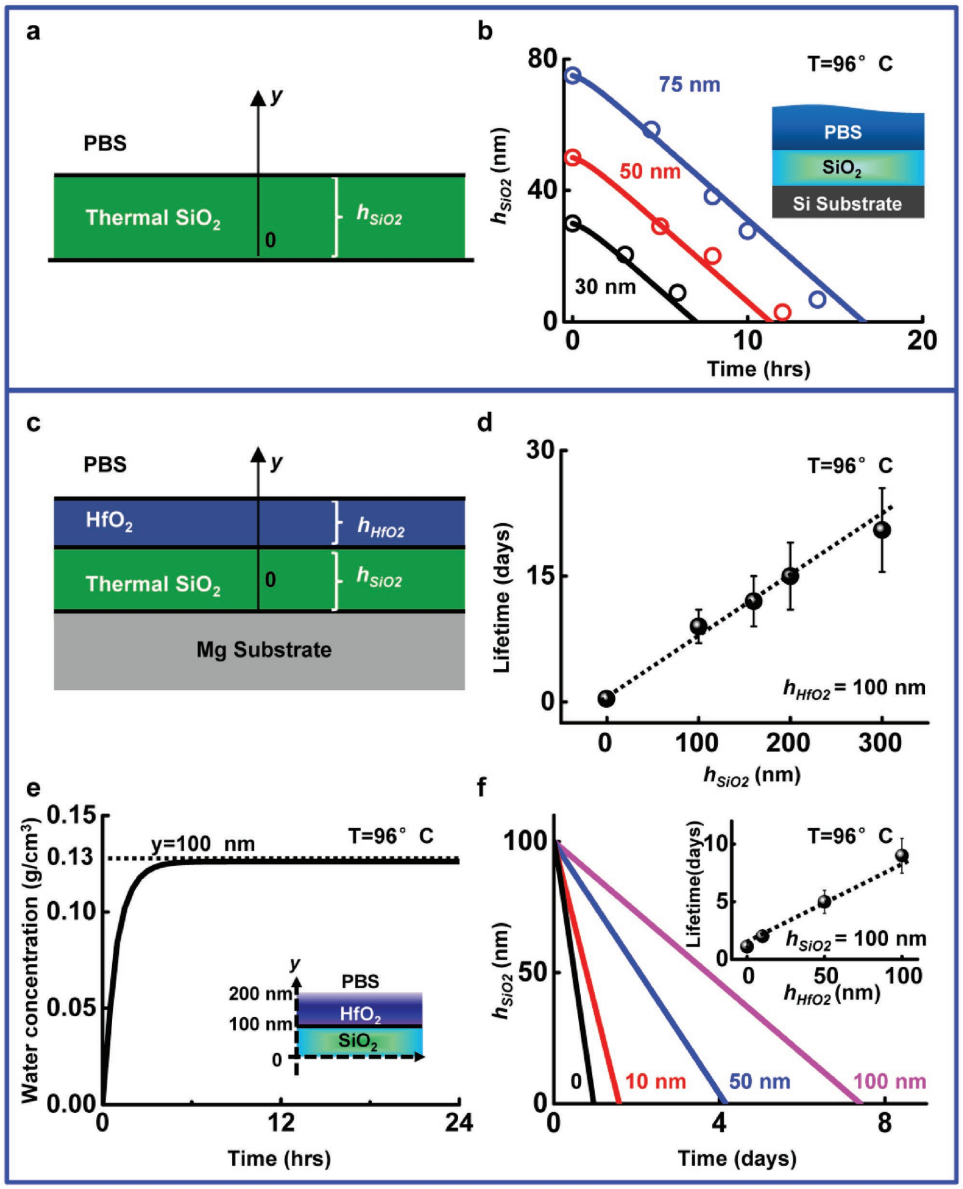

Figure 3. Theoretical modeling of reactive diffusion for the hydrolysis of thermal SiO_2 and HfO_2/SiO_2 barriers. a) Schematic illustration of the single-layer model. b) Simulated (lines) and measured (symbols) changes in thickness of a single layer of thermal SiO_2 with initial thicknesses of 30, 50, and 75 nm in PBS solution at 96 °C. c) Schematic illustration of the bilayer model. d) Simulated (line) and measured (symbols) lifetime of a HfO_2/SiO_2 bilayer barrier with a 100-nm-thick layer of HfO_2 and different thicknesses of thermal SiO_2. e) Distribution of water concentration at the interface of a 100-nm/100-nm-thick bilayer of HfO_2/SiO_2 barrier. f) Changes in thickness of thermal SiO_2 in a HfO_2/SiO_2 bilayer barrier with a 100-nm-thick layer of SiO_2 and HfO_2 with initial thicknesses of 0, 10, 50, and 100 nm. The inset presents the simulated (line) and measured (symbols) lifetime of a HfO_2/SiO_2 bilayer barrier with a 100-nm-thick layer of SiO_2 and different thicknesses of HfO_2 (0, 10, 50, and 100 nm).

different polymer capping materials on thermal SiO_2, the soak tests in Table S1 (Supporting Information) yield the polymer diffusivities, for example, $D_{SU\text{-}8} = 7 \times 10^{-15}$ cm^2 s^{-1}, $D_{PI} = 5.5 \times 10^{-15}$ cm^2 s^{-1}. The detailed simulated results of polymer/SiO_2 barriers appear in the Appendix and Figure S7 (Supporting Information). The findings clearly indicate that the low water diffusivity of HfO_2 makes it superior to all examined polymers. Figure 3d predicts the bilayer barrier lifetime as a function of the initial thermal SiO_2 thickness, for the case of a 100-nm-thick HfO_2 layer. The simulated results (line) agree well with those measured (symbols). Figure 3e shows the water concentration as a function of time at the interface ($y = 100$ nm) of a 100/100 nm bilayer of HfO_2/SiO_2. The water concentration gradually reaches saturation at ≈0.13 g cm^{-3} at the HfO_2/SiO_2 interface after ≈3 h, revealing a fast equilibrium between reaction and diffusion. Here, HfO_2 serves as a passive layer to effectively mitigate the dissolution of the underlying SiO_2.

Figure 3f shows the changes in thickness of the SiO_2 in a bilayer barrier of HfO_2/SiO_2 with a 100-nm-thick layer of SiO_2 and HfO_2 with initial thicknesses of 0, 10, 50, and 100 nm. The lifetime as a function of the initial HfO_2 thickness appears in the inset. The simulated results (line) show good agreement

with those measured (symbols). The temperature-dependent lifetimes are also investigated. With D_{HfO_2} at 96 °C, the diffusivities at different temperatures can be determined according to the Arrhenius scaling, thus giving the lifetime as a function of temperature (Appendix and Figure S8, Supporting Information) by Equation (6). Specifically, a bilayer barrier of HfO_2/SiO_2 (100/100 nm thick) offers a projected lifetime of over 40 years at 37 °C PBS (pH of 7.4).

The enhanced lifetime indicates that the HfO_2 capping layer effectively delays the permeation of biofluid to the underlying SiO_2. Since biofluids contain not only water molecules but alkali metal ions that are known to accelerate the SiO_2 dissolution, parametric studies of different ionic concentrations provide additional insights into the underlying chemistry. **Figure 4** describes the ion effect on the dissolution of SiO_2 and its lifetime with/without HfO_2 capping layer. The solutions use 10×10^{-3} M Tris to adjust the pH to a physiological condition, pH 7.4. Figure 4a summarizes changes in the reflectance of a 320-nm-thick single layer of thermal SiO_2 on a silicon wafer after soaking in different solutions with different concentrations of sodium chloride (NaCl), indicative of various $[Na^+]$, for 14 h at 96 °C. The uniform color distributions are consistent with macroscopically uniform rates of dissolution for all values of $[Na^+]$. The peaks of the reflectance curves in Figure 4a shift toward shorter wavelengths as the thicknesses decreases. The rates for these shifts increase with concentration, thereby demonstrating the catalyzing effect of Na^+ on dissolution. Previous studies show that alkali and alkaline metal ions accelerate the dissolution of quartz and other amorphous silica polymorphs in near-neutral pH solutions.[37–42] As an example for the systems studied here, Figure 4b shows similar soaking results in solutions containing Ca^{2+}. Here, 0.047 and 0.333 M calcium chloride ($CaCl_2$) concentrations yield ionic strengths similar to those of the 0.14 and 1 M NaCl solutions in Figure 4a. The dissolution behavior depends more strongly on $[Ca^{2+}]$, than $[Na^+]$ at the same ionic strength. Figure 4c summarizes the dissolution rates of thermal SiO_2 in solutions with various values of $[Na^+]$ and $[Ca^{2+}]$, quantitatively determined from the reflectance data in Figure 4a,b. The results indicate that the presence of Ca^{2+} could determine the lifetime of the SiO_2 layer even when its concentration is lower than that of Na^+. According to studies in the literature, cations facilitate deprotonation of −OH groups on the surface of SiO_2 by shielding negative charges, as supported by empirical rate laws that indicate an increase in dissolution rates with surface charge.[40,41,43] Other experimental and computational evidence suggest that cations can modify the interfacial water structure to promote hydrolysis of Si−O−Si bonds.[39,42]

Figure 4d shows results of experiments on the lifetimes of a 100-nm-thick layer of thermal SiO_2 with/without an HfO_2 capping layer, all in the presence of ions. The two dotted curves correspond to lifetimes in Na^+ (black) and Ca^{2+} (red) containing

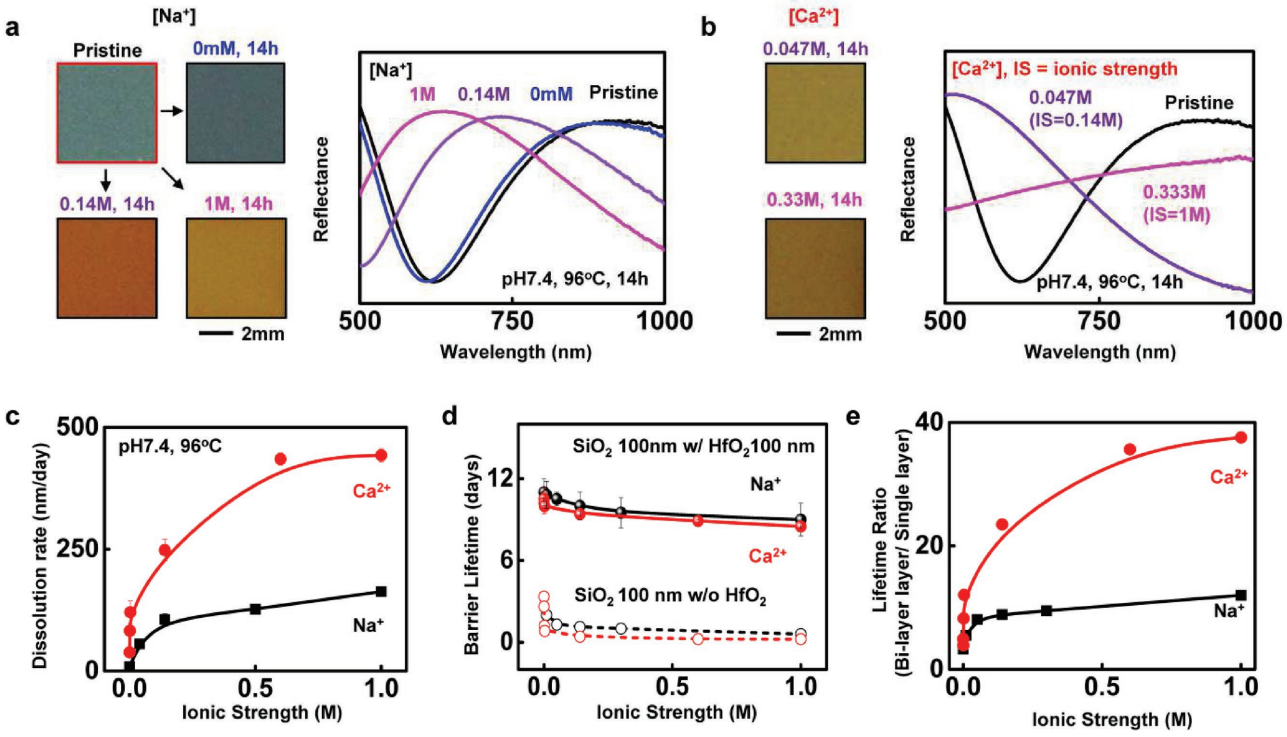

Figure 4. Ion effect on SiO_2 dissolution and lifetimes for thermally grown SiO_2 with/without a capping layer of HfO_2. a) Optical properties of a 320-nm-thick layer of thermal SiO_2 after soaking in solutions with various $[Na^+]$. Optical images (left) and reflectance (right) of the SiO_2. b) Optical properties of the same SiO_2 layer after soaking in solutions with various $[Ca^{2+}]$. c) Dissolution rates for a single layer of SiO_2 in solutions containing Na^+ and Ca^{2+}. d) Lifetime of barrier layer of SiO_2 (100-nm thick) with and without a capping layer of HfO_2 (100-nm thick) in solutions with various $[Na^+]$ and $[Ca^{2+}]$. e) Relative lifetime of a bilayer of HfO_2/SiO_2 with respect to a single layer of SiO_2 in solutions containing Na^+ and Ca^{2+}. Here, the ratios of the lifetimes between bilayer barriers and single-layer barriers are presented.

solutions. The results are consistent with the dissolution rates of SiO_2 (Figure 4c). The solid lines show prolonged lifetimes with the addition of the 100-nm-thick capping layer of HfO_2. As with the single layer of SiO_2 barrier, the results for HfO_2/SiO_2 barrier show longer lifetimes in Na^+ solutions than in Ca^{2+} solutions at the same ionic strength. Compared to 100-nm-thick layer of thermal SiO_2, the bilayer barrier of HfO_2/SiO_2 (100/100 nm thick) enhances the lifetime by a factor of ten. Figure 4e calculates the lifetime ratios between the bilayer of HfO_2/SiO_2 barrier (100/100 nm thick) and single layer of thermal SiO_2 barrier (100 nm thick) at each ionic strength. This ratio increases up to a certain level as the ionic strength increases. In the same context, the HfO_2/SiO_2 more strongly mitigates the diffusion of Ca^{2+} rather than Na^+, possibly due to a larger hydrated ionic radius and higher positive charge of Ca^{2+} compared to Na^+.[44]

In addition to their effects on dissolution, ions in biofluids (mostly positive species such as Na^+) that diffuse through the barriers can adversely affect the performance of underlying transistors, mainly by electrostatically shifting their threshold voltages (V_T).[45] Specifically, ion diffusion in PBS can accumulate a layer of positive ions (most Na^+) at the transistor channel, as schematically illustrated in **Figure 5**a, thus leading to an additional electric field that acts in concert with the gate voltage (V_G) at the transistor front gate. These positive ions give rise to a positive enhancement to V_G. As a result, the transistor switches on with a more negative V_G at the front gate, corresponding to a negative shift in V_T for an NMOS device. Ion drift-diffusion tests on encapsulated NMOS transistors (layer configuration shown in Figure 1d) allow comparisons of HfO_2/SiO_2 and SiO_2 as ion barriers. Results of accelerated soak tests of NMOS transistors during application of an external bias while immersed in PBS solution at 96 °C and pH of 7.4 are shown in Figure 5b,c. The bias (V_{app}, 3 V) exists between a platinum probe in the PBS solution and the transistor electrodes (source, drain, and gate), as illustrated in the insets. For present purposes, device failure is defined as the point when the shift in the threshold voltage ΔV_T reaches 1 V. The positive V_{app} serves as a driving force to impel positive ion transport through barriers, the result of which shifts V_T of transistors under a 200-nm-thick layer of SiO_2 barrier by electrostatic interactions with the Si channel, as shown in Figure 5b. As shown in Figure 5c, the key performance characteristics of transistors with bilayer barriers of HfO_2/SiO_2 (100/100 nm thick) remain constant in accelerated soak tests (in 96 °C PBS solution) over the full duration of the experiments. The results demonstrate that the bilayer of HfO_2/SiO_2 barriers can effectively retard ion diffusion process compared to the single layer of SiO_2 barriers.

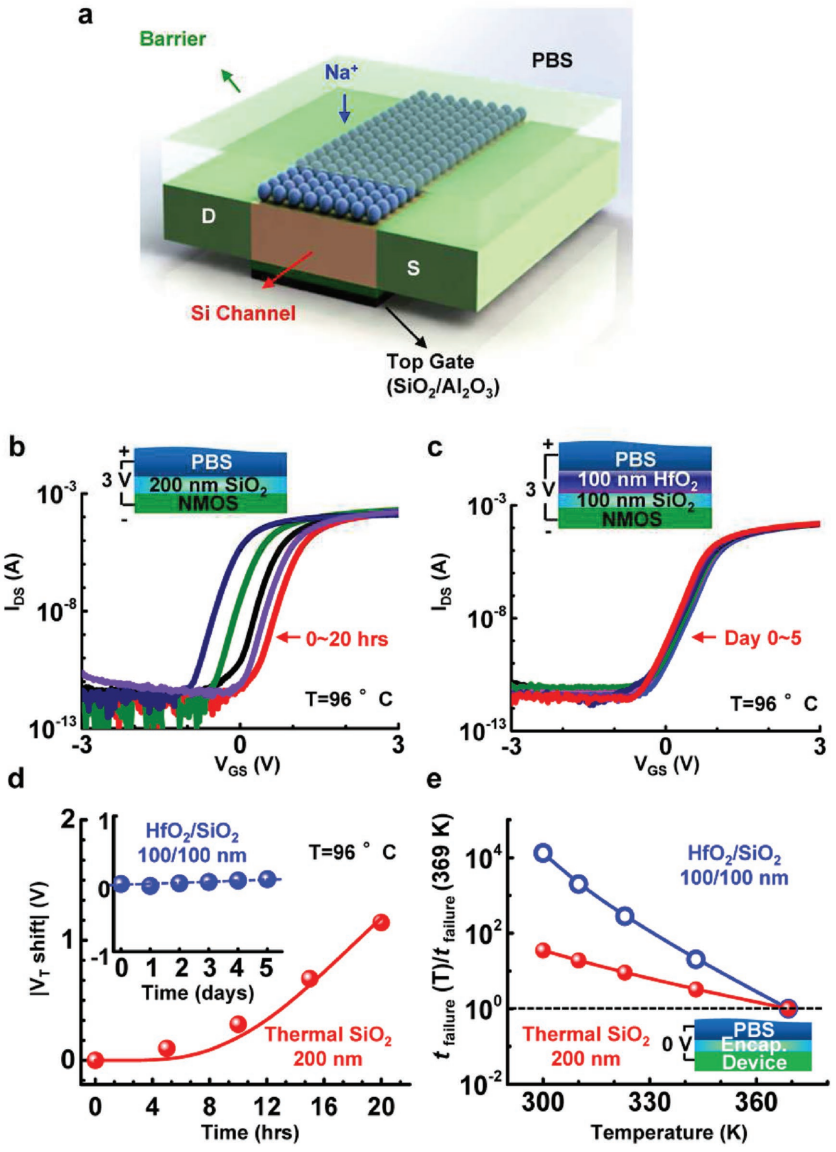

Figure 5. Experimental and simulation results for the behavior of NMOS transistors encapsulated with SiO_2 and HfO_2/SiO_2 barriers in various tests of immersion in PBS solution at pH 7.4 and 96 °C. a) Cross-sectional illustration of the embedded MOSFET device with sodium in the channel region. Results of tests for b) a 200-nm-thick layer of SiO_2 and c) a 100/100-nm-thick bilayer of HfO_2/SiO_2 in PBS soak tests at 96 °C and with an applied bias, $V_{app} = 3$ V. Schematic illustrations of the samples and bias configurations appear in the upper insets. d) Shift in the threshold voltage as a function of time with $V_{app} = 3$ V bias for a 200-nm-thick layer of SiO_2 at 96 °C. The solid dots are experimental data and the lines are simulations. Inset indicates shifts in threshold voltage for a 100/100 nm bilayer of HfO_2/SiO_2 as a function of time with $V_{app} = 3$ V bias at 96 °C. e) Acceleration factors for both ion diffusion and dissolution as a function of temperature for a 200-nm-thick layer of SiO_2 and a 100/100 nm bilayer of HfO_2/SiO_2, respectively. The inset offers a schematic illustration of the geometry.

Results of modeling of Na^+ transport processes appear in Figure 5d,e. Here, Figure 5d shows the shift in V_T extracted from Figure 5b for a 200-nm-thick layer of SiO_2 within 1 d with

V_{app} = 3 V at T = 96 °C. The drift diffusion is closely related to the layer of surface charge density Q_s of Na^+ located at the thermal SiO_2/substrate Si interface (Appendix and Figure S9, Supporting Information). To find the relationship between Q_s and ΔV_T, we numerically simulate a 2D NMOS transistor with commercial software (Sentaurus Technology Computer Aided Design) using experimentally determined device parameters. The numerical result predicted by this model (red solid lines) fits well with experimental data (red solid dots), as displayed in Figure 5d. Corresponding calculation details appear in the Appendix (Supporting Information). The inset of Figure 5d presents values of ΔV_T extracted from data in Figure 5c with a 100/100-nm-thick bilayer of HfO_2/SiO_2 barrier. Here, the shifts in V_T are extraordinarily small (less than ≈0.05V) in all cases, which further support the outstanding properties of HfO_2/SiO_2 as bilayer ion barriers.

Modeling can also capture the competition between dissolution and ion diffusion in SiO_2 and HfO_2/SiO_2. Figure 5e presents such competition for a 200-nm-thick layer of thermal SiO_2 and a 100/100-nm-thick bilayer of HfO_2/SiO_2, respectively, both of which form on transistors. The inset of Figure 5e displays the configuration without V_{app}. We consider an acceleration factor (AF) for the failure time as a function of temperature, considering both dissolution and ion diffusion failures together. In all cases, device failure corresponds to the point when the SiO_2 disappears due to hydrolysis or when the shift in the threshold voltage ΔV_T reaches 1 V. The AF is defined as $t_{failure}(T)/t_{failure}$ (369 K), normalized at 369 K. The temperature-dependent Na^+ diffusion coefficient follows an Arrhenius relationship: $D = D_0 \cdot e^{-E_A/kT}$, where k is the Boltzmann constant and T is temperature. D_0 is the pre-exponential factor and E_A is the activation energy. We extracted D_0 and E_A from the data of Figure 5d. For the single layer of SiO_2 barrier, ion penetration dominates the failure time, because the corresponding dissolution failure time is much longer than that of the ion-diffusion process. On the other hand, the bilayer of HfO_2/SiO_2 barrier offers improved ion-barrier properties. Here, dissolution plays an important role. The AF of HfO_2/SiO_2 (100/100 nm thick) uses the dissolution failure time from Figure 3d (369 K) and corresponding simulations for other temperatures in the Appendix and Figure S5 (Supporting Information). A bilayer of HfO_2/SiO_2 barrier offers a projected lifetime of over 40 years at 37 °C PBS (pH of 7.4), leading to a much higher AF (three orders of magnitude) than that of SiO_2, due to the enhanced ion-barrier properties.

3. Conclusion

In summary, the use of coatings of HfO_2 on top of ultrathin layers of SiO_2 thermally grown on device-grade silicon wafers can provide excellent water/ion barrier performance for flexible electronic devices. A comprehensive combination of experiments and simulations highlights the underlying physical and chemical effects associated with this type of bilayer barrier. Implementing these strategies in active flexible electronic and optoelectronic platforms will allow for a wide range of chronic studies in animals and, potentially, for use in advanced bioelectronic implants in humans.

4. Experimental Section

Details of fabrication steps, test structures, immersion studies at various ion concentrations and temperatures, theoretical analysis including reactive diffusion models and sodium-ion transport appear in the Appendix (Supporting Information).

Supporting Information

Supporting Information is available from the Wiley Online Library or from the author.

Acknowledgements

E.S., Y.K.L., R.L., and J.L. contributed equally to this work. This work was supported by Defense Advanced Research Projects Agency Contract HR0011-14-C-0102, and the Center for Bio-Integrated Electronics. The authors acknowledge the use of facilities in the Micro and Nanotechnology Laboratory for device fabrication and the Frederick Seitz Materials Research Laboratory for Advanced Science and Technology for device measurement at the University of Illinois at Urbana–Champaign. E.S. acknowledges support from China Scholarship Council. R.L. acknowledges the support from the Young Elite Scientist Sponsorship Program by China Association for Science and Technology (CAST). Z.X. acknowledges the support National Natural Science Foundation of China (Grant No. 11402134). Y.H. acknowledges the support from NSF (Grant Nos. DMR-1121262, CMMI-1400169, and CMMI-1534120) and the NIH (Grant No. R01EB019337). M.A. acknowledges the support from NSF Nano-biosensing Program Grant No. 1403582 and NSF NCNNEEDS Program under Grant No. 1227020-EEC.

Conflict of Interest

The authors declare no conflict of interest.

Keywords

biofluids, hafnium oxide, hermetic packaging, silicon dioxide, water-and-ion barriers

Received: April 28, 2017
Revised: June 1, 2017
Published online: July 20, 2017

[1] J.-W. Jeong, J. G. McCall, G. Shin, Y. Zhang, R. Al-Hasani, M. Kim, S. Li, J. Y. Sim, K. I. Jang, Y. Shi, D. Y. Hong, Y. Liu, G. P. Schmitz, L. Xia, Z. He, P. Gamble, W. Z. Ray, Y. Huang, M. R. Bruchas, J. A. Rogers, *Cell* **2015**, *162*, 662.
[2] K. L. Montgomery, A. J. Yeh, J. S. Ho, V. Tsao, S. M. Iyer, L. Grosenick, E. A. Ferenczi, Y. Tanabe, K. Deisseroth, S. L. Delp, A. S. Y. Poon, *Nat. Methods* **2015**, *12*, 969.
[3] T. Kim, J. G. McCall, Y. H. Jung, X. Huang, E. R. Siuda, Y. Li, J. Song, Y. M. Song, H. A. Pao, R.-H. Kim, C. Lu, S. D. Lee, I.-S. Song, G. Shin, R. Al-Hasani, S. Kim, M. P. Tan, Y. Huang, F. G. Omenetto, J. A. Rogers, M. R. Bruchas, *Science* **2013**, *340*, 211.
[4] A. Canales, X. Jia, U. P. Froriep, R. A. Koppes, C. M. Tringides, J. Selvidge, C. Lu, C. Hou, L. Wei, Y. Fink, P. Anikeeva, *Nat. Biotechnol.* **2015**, *33*, 277.
[5] J. Viventi, D.-H. Kim, J. D. Moss, Y.-S. Kim, J. A. Blanco, N. Annetta, A. Hicks, J. L. Xiao, Y. Huang, D. J. Callans, J. A. Rogers, B. Litt, *Sci. Transl. Med.* **2010**, *2*, 24ra22.

[6] D.-H. Kim, N. S. Lu, R. Ghaffari, Y.-S. Kim, S. P. Lee, L. Xu, J. Wu, R.-H. Kim, J. Song, Z. Liu, J. Viventi, B. d. Graff, B. Elolampi, M. Mansour, M. J. Slepian, S. Hwang, J. D. Moss, S.-M. Won, Y. Huang, B. Litt, J. A. Rogers, *Nat. Mater.* **2011**, *10*, 316.
[7] L. Xu, S. R. Gutbrod, A. P. Bonifas, Y. Su, M. S. Sulkin, N. Lu, H.-J. Chung, K.-I. Jang, Z. Liu, M. Ying, C. Lu, R. C. Webb, J.-S. Kim, J. I. Laughner, H. Cheng, Y. Liu, A. Ameen, J.-W. Jeong, G.-T. Kim, Y. Huang, I. R. Efimov, J. A. Rogers, *Nat. Commun.* **2014**, *5*, 3329.
[8] D.-H. Kim, R. Ghaffari, N. Lu, S. Wang, S. P. Lee, H. Keum, R. D'Angelo, L. Klinker, Y. Su, C. Lu, Y.-S. Kim, A. Ameen, Y. Li, Y. Zhang, B. d. Graff, Y.-Y. Hsu, Z. Liu, J. Ruskin, L. Xu, C. Lu, F. G. Omenetto, Y. Huang, M. Mansour, M. J. Slepian, J. A. Rogers, *Proc. Natl. Acad. Sci. USA* **2012**, *109*, 19910.
[9] X. Dai, W. Zhou, T. Gao, J. Liu, C. M. Lieber, *Nat. Nanotechnol.* **2016**, *11*, 776.
[10] B. Tian, T. Cohen-Karni, Q. Qing, X. J. Duan, P. Xie, C. M. Lieber, *Science* **2010**, *329*, 830.
[11] R. Nawrocki, N. Matsuhisa, T. Yokota, T. Someya, *Adv. Electron. Mater.* **2015**, *2*, 1.
[12] D.-H. Kim, N. Lu, R. Ma, Y.-S. Kim, R.-H. Kim, S. Wang, J. Wu, S. M. Won, H. Tao, A. Islam, K. J. Yu, T.-I. Kim, R. Chowdhury, M. Ying, L. Xu, M. Li, H.-J. Chung, H. Keum, M. McCormick, P. Liu, Y.-W. Zhang, F. G. Omenetto, Y. Huang, T. Coleman, J. A. Rogers, *Science* **2011**, *333*, 838.
[13] D. J. Lipomi, M. Vosgueritchian, B. C. Tee, S. L. Hellstrom, J. A. Lee, C. H. Fox, Z. Bao, *Nat. Nanotechnol.* **2011**, *6*, 788.
[14] M. C. McAlpine, H. Ahmad, D. Wang, J. R. Heath, *Nat. Mater.* **2007**, *6*, 379.
[15] W. Gao, S. Emaminejad, H. Y. Nyein, S. Challa, K. Chen, A. Peck, H. M. Fahad, H. Ota, H. Shiraki, D. Kiriya, D. H. Lien, G. A. Brooks, R. W. Davis, A. Javey, *Nature* **2016**, *529*, 509.
[16] W. Wu, L. Wang, Y. Li, F. Zhang, L. Lin, S. Niu, D. Chenet, X. Zhang, Y. Hao, T. F. Heinz, J. Hone, Z. L. Wang, *Nature* **2014**, *514*, 470.
[17] S. Xu, Y. Zhang, L. Jia, K. E. Mathewson, K. I. Jang, J. Kim, H. Fu, X. Huang, P. Chava, R. Wang, S. Bhole, L. Wang, Y. J. Na, Y. Guan, M. Flavin, Z. Han, Y. Huang, J. A. Rogers, *Science* **2014**, *344*, 70.
[18] M. Kaltenbrunner, T. Sekitani, J. Reeder, T. Yokota, K. Kuribara, T. Tokuhara, M. Drack, R. Schwödiauer, I. Graz, S. Bauer-Gogonea, S. Bauer, T. Someya, *Nature* **2013**, *499*, 458.
[19] C. M. Lochner, Y. Khan, A. Pierre, A. C. Arias, *Nat. Commun.* **2014**, *5*, 5745.
[20] D. Son, J. Lee, S. Qiao, R. Ghaffari, J. Kim, J. E. Lee, C. Song, S. J. Kim, D. J. Lee, S. W. Jun, S. Yang, M. Park, J. Shin, K. Do, M. Lee, K. Kang, C. S. Hwang, N. Lu, T. Hyeon, D.-H. Kim, *Nat. Nanotechnol.* **2014**, *9*, 397.
[21] N. T. Kalyani, S. J. Dhoble, *Renewable Sustainable Energy Rev.* **2015**, *44*, 319.
[22] L. Bowman, J. D. Meindl, *IEEE Trans. Biomed. Eng.* **1986**, *BME-33*, 248.
[23] J.-S. Park, H. Chae, H. K. Chung, S. I. Lee, *Semicond. Sci. Technol.* **2011**, *26*, 034001.
[24] H. S. Mayberg, A. M. Lozano, V. Voon, H. E. McNeely, D. Seminowicz, C. Hamani, J. M. Schwalb, S. H. Kennedy, *Neuron* **2005**, *45*, 651.
[25] B. S. Wilson, C. C. Finley, D. T. Lawson, R. D. Wolford, D. K. Eddington, W. M. Rabinowitz, *Nature* **1991**, *352*, 236.
[26] R. S. Sanders, M. T. Lee, *Proc. IEEE* **1996**, *84*, 480.
[27] J. Ahmad, K. Bazaka, L. J. Anderson, R. D. White, M. V. Jacob, *Renewable Sustainable Energy Rev.* **2013**, *27*, 104.
[28] H. Fang, J. Zhao, K. J. Yu, E. Song, A. B. Farimani, C.-H. Chiange, X. Jin, Y. Xue, D. Xu, W. Dui, K. J. Seo, Y. Zhong, Z. Yang, S. M. Won, G. Fang, S. W. Choi, S. Chaudhuri, Y. Huang, M. A. Alam, J. Viventi, N. R. Aluru, J. A. Rogers, *Proc. Natl. Acad. Sci. USA* **2016**, *113*, 11682.
[29] H. Fang, K. J. Yu, C. Gloschat, Z. Yang, E. Song, C.-H. Chiang, J. Zhao, S. M. Won, S. Xu, M. Trumpis, Y. Zhong, S. W. Han, Y. Xue, D. Xu, S.W. Choi, G. Cauwenberghs, M. Kay, Y. Huang, J. Viventi, I. R. Efimov, J. A. Rogers, *Nat. Biomed. Eng.* **2017**, *1*, 0038.
[30] S.-K. Kang, S.-W. Hwang, H. Cheng, S. Yu, B. H. Kim, J.-H. Kim, Y. Huang, J. A. Rogers, *Adv. Funct. Mater.* **2014**, *24*, 4427.
[31] M. Schindler, S. K. Kim, C. S. Hwang, C. Schindler, A. Offenhäusser, S. Ingebrandt, *Phys. Status Solidi RRL* **2008**, *2*, 4.
[32] L. Maggiorella, G. Barouch, C. Devaux, A. Pottier, E. Deutsch, J. Bourhis, E. Borghi, L. Levy, *Future Oncol.* **2012**, *8*, 1167.
[33] R. Li, H. Cheng, Y. Su, S.-W. Hwang, L. Yin, H. Tao, M. A. Brenckle, D.-H. Kim, F. G. Omenetto, J. A. Rogers, Y. Huang, *Adv. Funct. Mater.* **2013**, *23*, 3106.
[34] P. V. Danckwerts, *Trans. Faraday Soc.* **1950**, *46*, 300.
[35] K. M. Davis, M. Tomozawa, *J. Non-Cryst. Solids* **1995**, *185*, 203.
[36] M. Tomozawa, K. M. Davis, *Mater. Sci. Eng.* **1999**, *A272*, 114.
[37] J. D. Rimstidt, *Geochim. Cosmochim. Acta* **2015**, *167*, 195.
[38] P. M. Dove, N. Han, J. J. De Yoreo, *Proc. Natl. Acad. Sci. USA* **2005**, *102*, 15357.
[39] P. M. Dove, D. A. Crerar, *Geochim. Cosmochim. Acta* **1990**, *54*, 955.
[40] P. V. Brady, J. V. Walther, *Chem. Geol.* **1990**, *82*, 253.
[41] M. Karlsson, C. Craven, P. M. Dove, W. H. Casey, *Aquat. Geochem.* **2001**, *7*, 13.
[42] O. Majérus, T. Gérardin, G. Manolescu, P. Barboux, D. Caurant, *Phys. Chem. Glasses: Eur. J. Glass Sci. Technol., Part B* **2014**, *13*, 261.
[43] K. C. Jena, P. A. Covert, D. K. Hore, *J. Phys. Chem. Lett.* **2011**, *2*, 1056.
[44] P. M. Dove, C. J. Nix, *Geochim. Cosmochim. Acta* **1997**, *61*, 3329.
[45] S. M. Sze, *Semiconductor Devices: Physics and Technology*, 2nd ed., John Wiley & Sons, Hoboken, NJ, **2008**.